EUROFUSION WPMST1-PR(16) 15388

P Piovesan et al.

Impact of ideal MHD stability limits on high-beta hybrid operation

Preprint of Paper to be submitted for publication in
43rd European Physical Society Conference on Plasma Physics (EPS)

This work has been carried out within the framework of the EUROfusion Consortium and has received funding from the Euratom research and training programme 2014-2018 under grant agreement No 633053. The views and opinions expressed herein do not necessarily reflect those of the European Commission.

Impact of ideal MHD stability limits on high-beta hybrid operation

P. Piovesan[1], V. Igochine[2], F. Turco[3], D.A. Ryan[4], M.R. Cianciosa[5], Y.Q. Liu[6], L. Marrelli[1], D. Terranova[1], R.S. Wilcox[7], A. Wingen[5], C. Angioni[2], A. Bock[2], C. Chrystal[7], I. Classen[8], M. Dunne[2], N.M. Ferraro[9], R. Fischer[2], A. Gude[2], C.T. Holcomb[10], P. Lauber[2], T.C. Luce[11], M. Maraschek[2], R. McDermott[2], T. Odstrčil[2], C. Paz-Soldan[11], M. Reich[2], M. Sertoli[2], W. Suttrop[2], N.Z. Taylor[7], M. Weiland[2], M. Willensdorfer[2], the ASDEX Upgrade Team, the DIII-D Team, and the EUROfusion MST1 Team*

1 Consorzio RFX, Corso Stati Uniti 4, I-35127 Padova, Italy
2 Max-Planck-Institut für Plasmaphysik, D-85748 Garching, Germany
3 Department of Applied Physics and Applied Mathematics, Columbia University, New York, NY 10027, USA
4 Department of Physics, University of York, Heslington, York, YO10 5DD, UK
5 Oak Ridge National Laboratory, Oak Ridge, TN, USA
6 CCFE, Culham Science Centre, Abingdon, OX14 3DB, UK
7 Oak Ridge Associated Universities, PO Box 117, Oak Ridge, TN 37831, USA
8 DIFFER, Nieuwegein, The Netherlands
9 Princeton Plasma Physics Laboratory, Princeton, New Jersey 08543, USA
10 Lawrence Livermore National Laboratory, Livermore, California 94550, USA
11 General Atomics, PO Box 85608, San Diego, California 92186-5608, USA
∗ See http://www.euro-fusionscipub.org/mst1

E-mail: paolo.piovesan@igi.cnr.it

Abstract. The hybrid scenario is a candidate for stationary high-fusion gain tokamak operation in ITER and DEMO. To obtain such performance, the energy confinement and the normalized pressure β_N must be maximized, which requires operating near or above ideal MHD no-wall limits. New experimental findings show how these limits can affect hybrid operation. Even if hybrids are mainly limited by tearing modes, proximity to the no-wall limit leads to 3D field amplification that affects plasma profiles, e.g. rotation braking is observed in ASDEX Upgrade throughout the plasma and peaks in the core. As a result, even the small ASDEX Upgrade error fields are amplified and their effects become visible. To quantify such effects, ASDEX Upgrade measured the response to 3D fields applied by 8×2 non-axisymmetric coils as β_N approaches the no-wall limit. The full $n = 1$ response profile and poloidal structure are measured by a suite of diagnostics and compared with linear MHD simulations, revealing a characteristic feature of hybrids: the $n = 1$ response is due to a global, marginally-stable $n = 1$ kink characterized by a large $m = 1, n = 1$ core harmonic due to q_{min} being just above 1. A helical core distortion of a few *cm* forms and affects various core quantities, including plasma rotation, electron and ion temperature, and intrinsic W density. In similar experiments, DIII-D also measured the effect of this helical core on the internal current profile, providing useful information to understand the physics of magnetic flux pumping, i.e. anomalous current redistribution by MHD modes that keeps $q_{min} > 1$. Thanks to flux pumping, a broad current profile is maintained in DIII-D even with large on-axis current drive, enabling fully non-inductive operation with high β_N up to $3.5 - 4$.

1. Introduction

To offer an attractive solution for energy production, tokamak operation must be optimized to reach high fusion gain in long-lasting, possibly steady state discharges. The so-called hybrid, or improved H-mode operational scenario is an excellent candidate in this direction [1, 2, 3, 4, 5, 6, 7]. Hybrid plasmas are characterized by a current profile broader than standard H-mode, a minimum safety factor just above unity, and thus by the absence of sawteeth. This is helped by a self-organized flux pumping mechanism provided by relatively benign MHD activity, which acts to redistribute central current [8, 9].

Removing the $q = 1$ surface makes $n = 1$ MHD activity more stable in general, including deleterious, possibly disruptive $n = 1$ tearing modes, which enables operation at higher normalized pressure, $\beta_N = \beta_T a B_T / I_P$, up to $3.5 - 4$ [7]. High β_N is key both to increase fusion power density and to reach long-lasting, or even steady state conditions, providing a relatively large bootstrap current fraction around $0.5 - 0.6$. Steady state operation in hybrid plasmas is ultimately made possible by the high efficiency of electron cyclotron current drive (ECCD) in the plasma center, combined with the redistribution of this central current provided by flux pumping [10, 11].

The requirement of maximizing β_N implies that hybrid plasmas must be operated near or even above the ideal MHD no-wall limit, the stability limit for ideal kink modes in absence of a stabilizing conducting wall, which normally occurs at $\beta_N \sim 3$ in this scenario. Though hybrid plasmas are mainly limited by tearing modes, as this scenario is optimized and β_N increases, the closeness to ideal MHD limits can introduce additional effects that impact the scenario. For example, external magnetic perturbations, whether they be intentionally applied to mitigate edge localized modes (ELM) or due to magnetic field errors in the machine, can be significantly amplified by the response of a marginally-stable kink mode already below the no-wall limit [12, 13]. For similar mechanisms, tearing and ideal instabilities can more easily couple near such limits, with tearing modes possibly becoming classically unstable when β_N approaches the ideal-wall limit [14, 15].

More attention to such effects was put before in plasmas with more advanced current profiles, characterized by higher q_{min} values and reversed magnetic shear, since in this case the no-wall limit can be encountered at even lower β_N [16, 17, 18, 19, 20, 21, 22]. We will show in this paper that similar effects can impact also the hybrid scenario at high-β_N. The consequences of operating near ideal MHD limits must be assessed and controlled to optimize this type of operation in present devices and in preparation of future machines like ITER and DEMO.

Recent experiments in the ASDEX Upgrade [23] and DIII-D [24] tokamaks have investigated these subjects. The results of these experiments are reported in this paper together with an extensive modelling effort done with the MHD stability codes MARS-F [25] and M3D-C^1 [26], the 3D equilibrium codes VMEC [27] and V3FIT [28], as well as with various transport codes. The MHD response was probed in hybrid plasmas at increasing β_N values by applying slowly rotating $n = 1$ fields, whose poloidal spectrum was systematically scanned thanks to the flexibility of the non-axisymmetric coil systems available in both machines. A wide set of diagnostics was used to measure with unprecedented detail the full radial and poloidal structure of the $n = 1$ plasma response in ASDEX Upgrade hybrid plasmas, also providing precious data to validate MHD codes, as reported in section 2. A significant helical core displacement forms in these plasmas in response to external $n = 1$ fields, which impacts both kinetic quantities, plasma rotation, and W density in the plasma core. The possible consequences on hybrid operation will be discussed in section 3, while observations of spontaneous kink and tearing modes is discussed in section 4. Section 5 reports plasma response measurements done in DIII-D hybrid plasmas using soft x-ray and internal magnetic field measurements based on the motional Stark effect (MSE). They were used to constrain the first 3D equilibrium reconstruction of a helical core equilibrium in a tokamak by the VMEC/V3FIT code. These results are useful to measure the impact of a helical core on the current profile and thus to better understand flux pumping physics. Conclusions and future perspectives are given in section 6.

2. Plasma response measurements and modelling in ASDEX Upgrade

The plasma response to slowly rotating (1 to $10Hz$) $n = 1$ magnetic perturbations was probed in ASDEX Upgrade hybrid plasmas as β_N is increased towards the

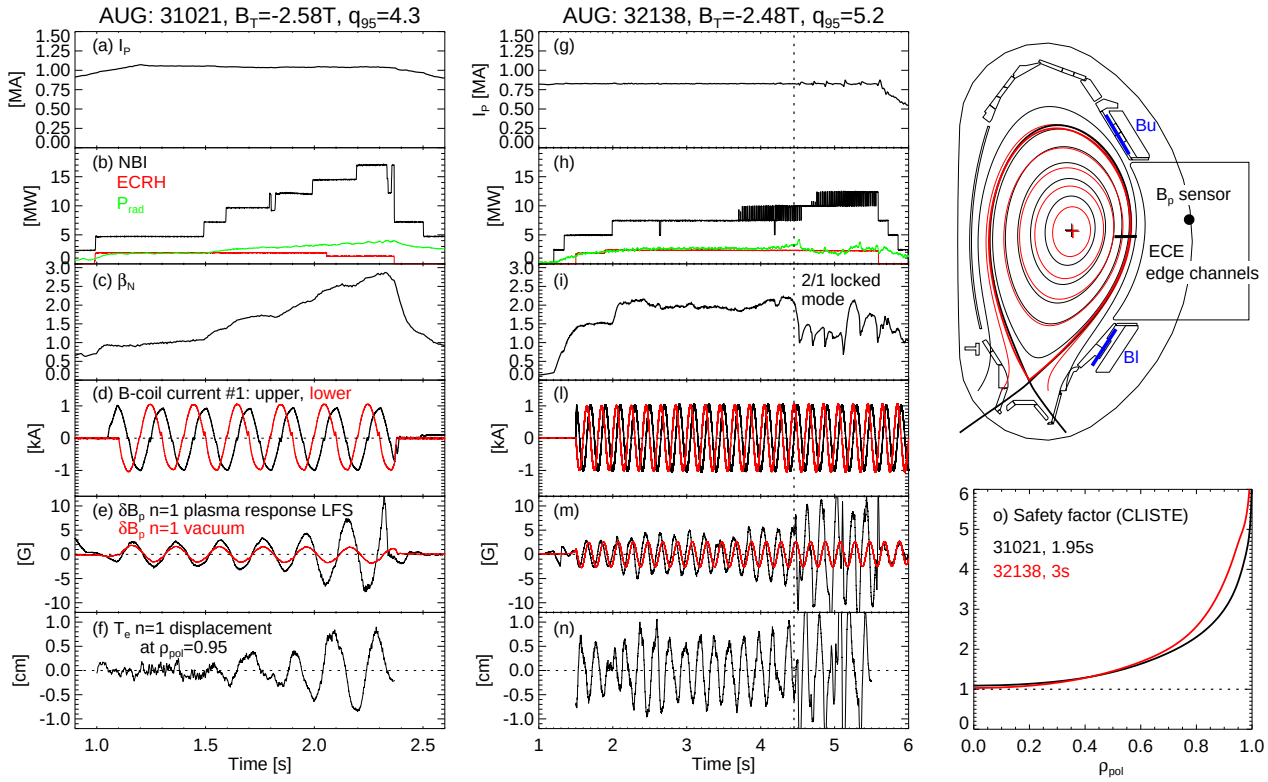

Figure 1. Two representative ASDEX Upgrade hybrid discharges, whose plasma response was probed with $n = 1$ fields rotating at $5Hz$: (a,g) plasma current; (b,h) NBI, EC and total radiation power; (c,i) normalized pressure, β_N; (d,l) current in upper and lower B-coil #1; (e,m) $n = 1$ plasma response and vacuum field measured by a couple of LFS B_p probes 180° apart; (f,n) $n = 1$ displacement at $\rho_{pol} = 0.95$ from ECE measurements, (o) safety factor profile. The right panel shows the shape of both discharges and the position of the B-coils (blue), the B_p probe and the ECE channels used to measure the edge response.

no-wall limit. The poloidal mode number spectrum of the applied $n = 1$ field was systematically scanned during these measurements thanks to the recent availability of new AC power supplies for the 8×2 internal non-axisymmetric coils, called B-coils, which makes this system a very flexible tool for these studies [29, 30]. The position of the upper and lower B-coils in the poloidal cross-section is shown in figure 1.

Two representative ASDEX Upgrade discharges studied in these experiments are described in figure 1. Discharge 31021, on the left column, is a high-current version of the hybrid scenario in ASDEX Upgrade with edge safety factor $q_{95} = 4.3$. Discharge 32138, on the central column, has lower plasma current and higher $q_{95} = 5.2$ and was recently developed to obtain non-inductive operation supported by neutral beam and ECCD [31]. In both cases β_N is gradually increased during the current flattop by ramping the neutral beam power, while central EC heating is applied to keep the core W concentration at acceptable values. A continuous 3/2 mode rotating at $15 - 20kHz$ is present in both discharges. The shape of the two discharges is similar, as shown in figure 1. The safety factor profiles shown in 1(o) were reconstructed by the CLISTE equilibrium code [32], using internal constraints like the radial location of the 3/2 mode, the position of the magnetic axis from ion temperature measurements that go across the plasma center, and the fast ion pressure calculated by TRANSP [33]. These equilibrium reconstructions have been used for the MHD modelling described in the following.

Slowly rotating ($5Hz$) $n = 1$ magnetic perturbations are applied with the B-coils during the β_N ramp to probe the plasma response. The poloidal spectrum of the applied field, which is determined by the relative phasing between the upper and lower B-coil rows, $\Delta\phi^{U/L}$, is kept here constant in time and is chosen in each discharge to maximize the alignment with the edge harmonics of the marginally-stable $n = 1$ kink mode, and thus its response. The optimum $\Delta\phi^{U/L}$ value changes with q_{95} and is $\Delta\phi^{U/L} \simeq 315°$ for discharge 31021, $\Delta\phi^{U/L} \simeq 90°$ for 32138, as determined by phasing scans performed in similar discharges and confirmed by MHD modelling. An example of such a scan will be reported in figure 5.

The $n = 1$ plasma response measured by a couple of poloidal magnetic field probes located near the LFS midplane is shown in figure 1(e) and (m). It

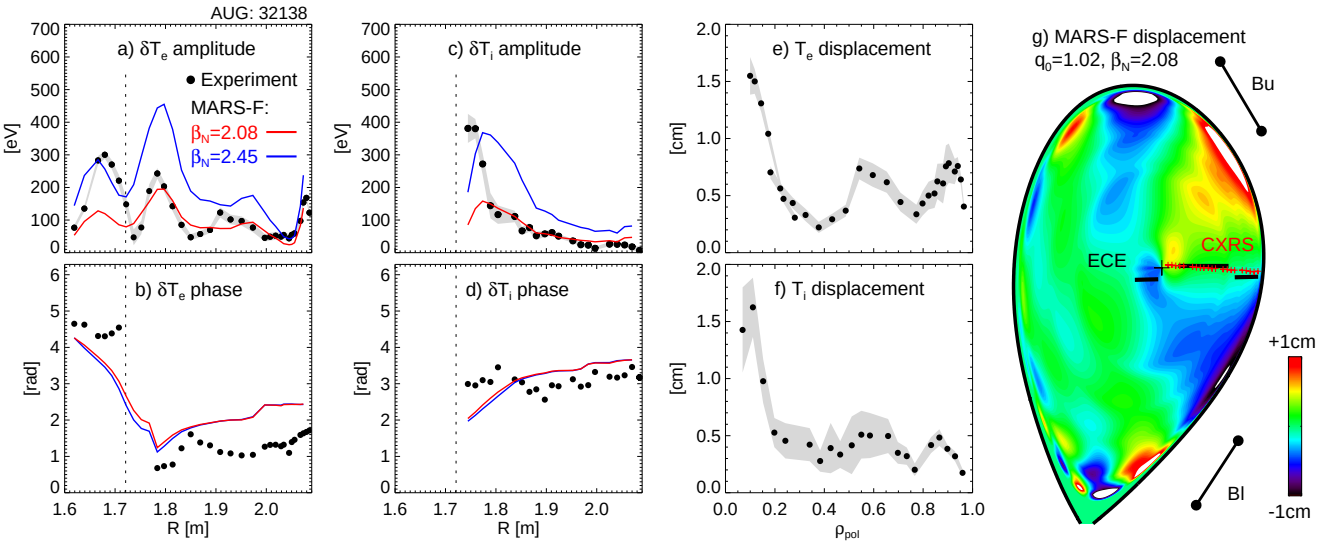

Figure 2. Radial profile of the plasma response to a rotating $n = 1$ field in ASDEX Upgrade discharge 32138: (a) amplitude and (b) phase of the T_e perturbation from ECE; (c) amplitude and (d) phase of the T_i perturbation from CXRS; and (e,f) the radial displacement profiles obtained from the perturbation profiles as $\xi_r = \delta T/(\partial T_0/\partial r)$. Black dots represent experimental data, red lines data simulated using the displacement predicted by MARS-F for this discharge, and blue lines a simulation with $\beta_N = 2.45$ higher that in experiment. Panel (g) shows a 2D map of the MARS-F displacement and the position of the ECE and CXRS channels.

increases as a function of β_N, indicating that the plasma is amplifying the applied $n = 1$ field. The $n = 1$ response is obtained from the difference of two time-integrated B_p probes toroidally separated by 180°, whose (R, z) position is indicated in figure 1. The B-coil $n = 1$ vacuum field, shown in red, was measured in dedicated dry shots and subtracted from the total B_p $n = 1$ field. Similar plasma amplification is observed in measurements of the edge plasma displacement at $\rho_{pol} = 0.95$ obtained from an electron cyclotron emission (ECE) diagnostic [34] as $\xi_r = \delta T_{rad}/(\partial T_{rad0}/\partial r)$. The location of the edge ECE channels is shown in figure 1. It was checked that in these plasmas and for the ECE channels used it is possible to assume $T_{rad} \simeq T_e$.

While the β_N ramp in discharge 31021 was intentionally stopped at $t \simeq 2.35s$ to avoid overheating of plasma facing components at this high level of injected power, the high-β_N phase in discharge 32138 was ended by a rotating $n = 1$ mode that appears at $t \simeq 4.35s$, locks after $0.1s$, and causes a β_N drop, as indicated by the vertical dotted line in figure 1. Analysis of fast ECE measurements (not shown) indicates that the mode initially has kink parity and, after about $50ms$, it develops an island at the $q = 2$ surface before locking to the wall. A similar transition from kink to tearing was also observed in other high-β_N discharges of this type and more details will be given in section 4. In the present case, the $n = 1$ mode does not seem to have a particular trigger, while in other cases its appearance is compatible with triggering by other MHD modes. Similar $n = 1$ modes are also observed when the rotation is significantly braked by external $n = 1$ fields, as will be shown in figure 5.

The radial profile of the $n = 1$ plasma response was measured in these plasmas using ECE measurements of the electron temperature profile, T_e, and charge exchange recombination spectroscopy (CXRS) measurements of the ion temperature profile, T_i, as reported in figure 2. The position of the ECE and CXRS channels are shown in panel (g). We consider here as an example discharge 32138 in the time interval $2.2 - 3.6s$. The amplitude and phase profiles of the T_e perturbation at the frequency of the applied $n = 1$ field are shown respectively in figures 2(a) and (b) with black dots. The fluctuation amplitude is finite everywhere, with two significant peaks in the core on opposite sides of the magnetic axis. Here the phase has a π-jump, which shows that the $n = 1$ response is dominated in the core by the $m = 1$ harmonic. The phase is rather constant across the plasma radius, compatible with an ideal nature of the $n = 1$ response. The T_i amplitude and phase profiles in figures 2(c) and (d) show similar results. They were obtained by the difference of T_i measurements from two CXRS systems toroidally separated by 180°, with channels at similar (R, z) positions in the poloidal cross-section. This particular diagnostic setup allows to extract $n = 1$ perturbations in a clean way, making sure that the T_i oscillations are not due to a global $n = 0$ oscillation of the entire profile, but really to a helical distortion of the plasma. Similar results based on line-integrated multi-

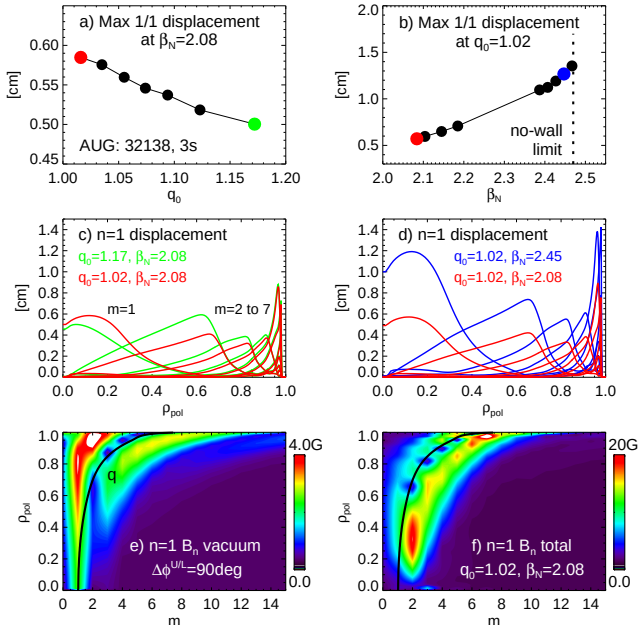

Figure 3. MARS-F results for ASDEX Upgrade discharge 32138: (a) Maximum $m = 1/n = 1$ displacement as a function of q_0 for a q_0 scan at constant $\beta_N = 2.08$ (experimental value). (b) Same for a β_N scan at constant $q_0 = 1.02$. (c,d) Displacement eigenfunctions for extreme q_0 and β_N values in the two scans. Poloidal mode number spectrum of (e) the $n = 1$ vacuum normal field and (f) of the total $n = 1$ normal field including plasma response for the MARS-F simulation marked in red in all panels and in figure 2.

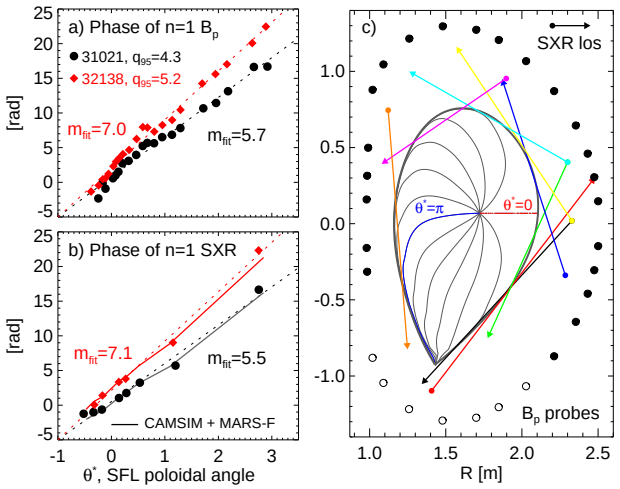

Figure 4. Relative phase of the $n = 1$ plasma response as a function of the straight-field-line poloidal angle, θ^*, measured in ASDEX Upgrade discharges 31021 (black) and 32138 (red) at different q_{95} by (a) two poloidal arrays of time-integrated B_p probes toroidally separated by 180° and (b) by all available soft x-ray chords almost tangent to the separatrix. Dashed lines represent a linear fit of the data and continuous lines in panel (b) soft x-ray data simulated using MARS-F eigenfunctions. The geometry of both diagnostics is shown in panel (c).

chord soft x-ray measurements were also documented before in similar ASDEX Upgrade discharges [35].

The profiles of the $n = 1$ displacement shown in figures 2(e) and (f) are obtained by dividing the T_e and T_i perturbation amplitudes by the gradients of the respective mean profiles. The displacement profiles given by the two diagnostics are remarkably similar. They are both dominated in the core by the $m = 1$ harmonic, which reaches displacement values around $1.5cm$. The smaller peaks at larger radii are compatible with higher-m harmonics, as it will be discussed in the following. The most interesting and new result of these measurements is that high-β_N hybrid plasmas in presence of external $n = 1$ fields tend to develop a helical core equilibrium, likely due to their q_{min} being just above 1. The same results were reproduced in DIII-D, as it is reported in section 5. A significant helical core deformation can have various consequences on hybrid operation, which are discussed in next section. It is interesting to notice that similar $n = 1$ helical core structures were observed to develop spontaneously in hybrid plasmas in JET [36, 37] and in the MAST spherical tokamak [38]. The difference and novelty of the present results is that the helical core is induced here by external 3D fields and it is not observed to form otherwise. The MHD modes normally present in these hybrid plasmas are 3/2 or 4/3 tearing modes or fishbones.

The plasma response was modelled using the linear MHD fluid code MARS-F [25] with the following experimental inputs: equilibrium from CLISTE, Spitzer resistivity, rotation profiles, and magnetic perturbations from B-coils. Since the B-coils are mounted on a massive copper conductor, called passive stabilizing loop, eddy currents induced during AC operation can modify the applied $n = 1$ field [30]. These effects were modelled with FEM electromagnetic calculations and included in our analysis: at $5Hz$ rotation frequency the amplitude is reduced by 40% and the phase is shifted by $-15°$. This correction is also included in the calculation of the upper-to-lower phasing, $\Delta\phi^{U/L}$, in figure 5. The MARS-F predictions obtained in this way are compared with the measured $n = 1$ response profiles by developing synthetic T_e and T_i diagnostics. The results are plotted with a red line in figure 2. A 2D contour plot of the MARS-F $n = 1$ radial displacement is shown in figure 2(g). Good agreement is found between experiment and simulation in the outer region of the plasma at radii $R > 1.8m$, as it will be also confirmed by edge measurements at multiple poloidal angles. But the large $m = 1$ peak in the core is not well matched.

To test the sensitivity of MARS-F predictions on the main kink mode drives, the input q and pressure profiles were scanned as summarized in figure

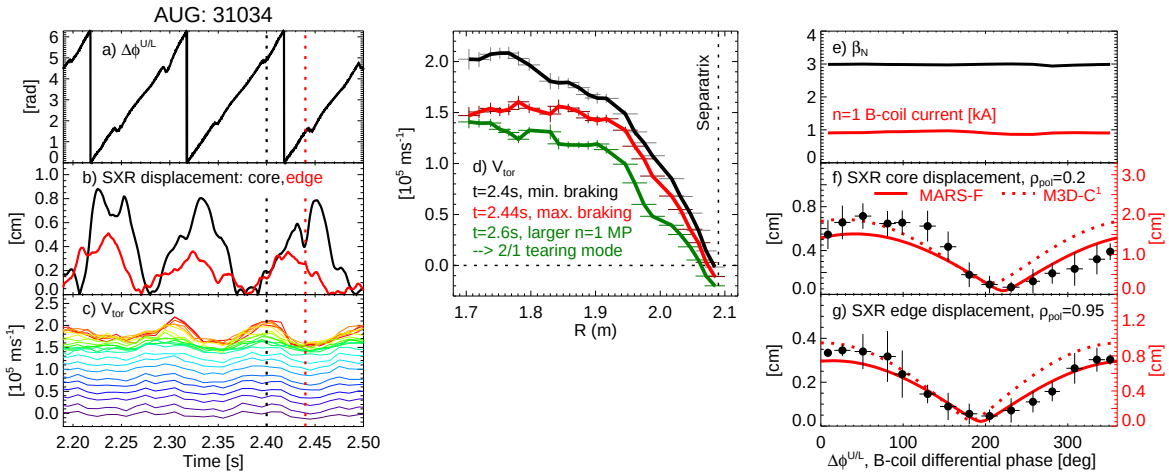

Figure 5. (a) Continuous scan of the upper-to-lower B-coil phasing in ASDEX Upgrade discharge 31034. (b) The $n = 1$ line-averaged soft x-ray displacement in the core (black) and edge region (red) peaks at a $\Delta\phi^{U/L}$ value that maximizes the coupling with the $n = 1$ kink. (c) Significant rotation braking occurs when the $n = 1$ response is maximum. (d) Rotation profiles at minimum and maximum braking show that the effect is largest in the core. The green profile represents a time with larger $n = 1$ field, just before an $n = 1$ rotating kink mode appears. (f) Core and (g) edge $n = 1$ displacement averaged over multiple $\Delta\phi^{U/L}$ scans and compared with MARS-F (continuous line) and M3D-C^1 predictions (dotted line).

3. The maximum 1/1 displacement is plotted in figure 3(a) as a function of the central safety factor, q_0. Here q_0 is varied in the uncertainty range of the CLISTE reconstruction, $q_0 = 1 - 1.2$, mainly due to lack of internal magnetic field constraints in these discharges. The 1/1 displacement slightly increases as q_0 approaches 1. The largest value is obtained at $q_0 = 1.02$, marked in red, corresponding to the simulation compared with experimental profiles in figure 2 (red line). The displacement eigenfunctions for the two extreme q_0 values in the scan are shown in green and red in figure 3(c). Changes in q_0 seem not to explain the discrepancy observed above. Larger displacement values are obtained by rescaling the whole pressure profile, and thus β_N, as shown in figure 3(b): all kink harmonics increase with β_N, as expected, and the kink mode becomes linearly unstable above $\beta_N = 2.47$, which provides an estimate of the no-wall limit. The simulation with $\beta_N = 2.45$ would give a 1/1 displacement of about $1.2cm$ similar to the experimental value, though the match at outer radii is obviously lost, as shown in figure 2 by a blue line. A better match between experiment and simulation may be obtained by local changes of the q and pressure profiles and/or by invoking physics beyond single-fluid MHD. To validate these effects, more precise measurements of the q and pressure profiles are necessary. These may be possible in future experiments thanks to the recent development of new imaging-MSE [40] and polarimetry diagnostics [41] in ASDEX Upgrade.

The m-spectrum of the vacuum $n = 1$ normal field applied to these plasmas is shown in figure 3(e) as a function of m and ρ_{pol}. The spectrum of the total normal field from MARS-F, which includes the plasma response, is shown in figure 3(f). Due to resonant field amplification, the total field is larger than the vacuum field by about a factor of 5 in the simulation with $\beta_N = 2.08$. Note that the larger harmonics are mainly non-resonant with respect to the q profile, with the core being dominated by the $m = 1$ harmonic and the edge by the $m = 7$ one.

The poloidal structure of the edge plasma response in the two discharges of figure 1 has been determined by magnetic and soft x-ray measurements at multiple poloidal angles, as shown in figure 4. The dominant m number was obtained by a linear fit of the phase delay between different channels as a function of the straight-field-line poloidal angle, which is evaluated here at $\rho_{pol} = 0.98$. In both cases, magnetic and soft x-ray measurements give consistent results: a dominant $m = 5-6$ in the lower $q_{95} = 4.3$ discharge and $m = 7$ in the higher $q_{95} = 5.2$ case. These values also agree with MARS-F predictions for both discharges, as confirmed also by simulations of the edge soft x-ray channels using a synthetic diagnostic described in [42], shown by a continuous line in figure 4(b).

To determine the $n = 1$ vacuum field spectrum that maximizes the plasma response, the upper-to-lower B-coil relative phasing, $\Delta\phi^{U/L}$, was continuously and slowly scanned in a single discharge, as anticipated above. This is shown in figure 5(a) for a discharge similar to discharge 31021 introduced above. The core and edge $n = 1$ response in figure 5(b) was measured by soft x-ray multi-chord cameras, as described in [35]. They both oscillate as $\Delta\phi^{U/L}$, and thus the

alignment of the applied $n = 1$ field with the edge harmonics of the $n = 1$ kink, vary in time. The CXRS plasma rotation measurements in figure 5(c) show that significant braking occurs when the $n = 1$ response peaks. The rotation profiles in figure 5 are taken at times of minimum (black) and maximum braking (red). The largest braking occurs in the core, which is consistent with the dominant 1/1 core response documented above. It is interesting to note that at a later time $t = 2.6s$ in this discharge, the applied $n = 1$ field was increased and the rotation profile was further reduced, as shown by the green line in figure 5(d). Simultaneously an $n = 1$ mode with kink parity appears rotating at $5 - 7kHz$. The mode transitions into a tearing mode after about $70ms$ and then it locks, causing a significant β_N drop. This observation reveals a possible dependence of the MHD stability of these plasmas on rotation, or rotation shear.

The dependence of the plasma response on the m-spectrum of the applied field agrees well with linear MHD predictions by both MARS-F and M3D-C^1. Figures 5(e) and (f) show as a function of $\Delta\phi^{U/L}$ the line-averaged soft x-ray $n = 1$ displacement measured in the core (chord tangency radius $\rho_{pol} = 0.2$) and at the edge ($\rho_{pol} = 0.95$), averaged over multiple phasing scans. The dependence of the MARS-F and M3D-C^1 displacement evaluated at the same radii agree well with experiment. The absolute values can not be directly compared, since soft x-ray measurements are line-averaged and tend to underestimate the displacement. These results indicate that the plasma responds as a single-mode rigid structure that extends from the edge to the core. The impact that such displacements have on various quantities, in particular in the core, is discussed in next section.

3. Impact of the helical core on kinetic profiles, rotation and W

As we have seen, the impact of the $n = 1$ plasma response in hybrid plasmas is not localized at the edge, where the $n = 1$ field is applied, but in the core. Here the largest field amplification occurs, though the external field is minimum. The impact of the helical core displacement on rotation profiles was evidenced in previous section. Here we will show that also other quantities can be significantly affected, with possible consequences on hybrid operation if these 3D distortions are not minimized, for example by error field correction. These results also offered the chance to probe interesting 3D physics effects.

Figure 6 shows the temporal evolution of various plasma quantities, including electron and ion temperature, rotation, electron and intrinsic W density, all measured near the magnetic axis, as a relatively low-

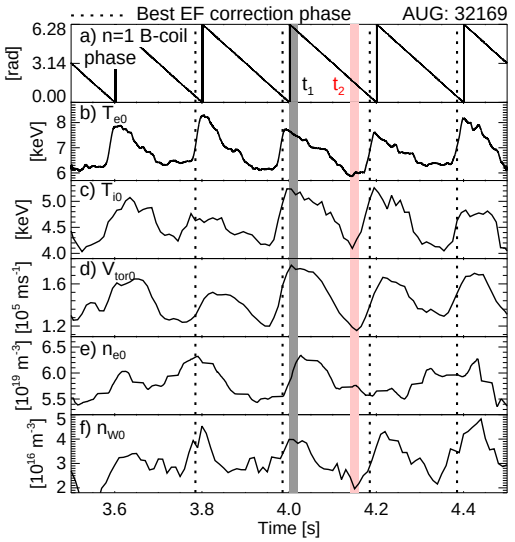

Figure 6. Temporal evolution of various quantities measured in the core as an $n = 1$ field applied by the B-coils is slowly rotated with amplitude comparable to the $n = 1$ error field in ASDEX Upgrade: (a) $n = 1$ upper B-coil phase, (b) electron and (c) ion temperature, (d) toroidal rotation, (e) electron density, and (f) W density. Vertical dotted lines indicate the B-coil phase for best error field correction. The upper-to-lower B-coil phasing $\Delta\phi^{U/L} = 90°$ is chosen to maximize the kink response.

amplitude, slowly roating $n = 1$ field is applied. In this discharge the $n = 1$ B-coil current is about 40% lower than in all cases discussed above. But quite surprisingly, though the applied field is lower, much larger variations in all core quantities are observed. These can not be explained by the helical displacement of the profiles: the core electron temperature, for example, varies by about $2keV$, while the perturbation amplitude due to the helical displacement would amount to a few $100eV$, as previously seen, and the same holds for the other quantities. The relatively low field applied here is comparable to the $n = 1$ machine error field, as determined by a compass scan approach in [43] and by independent measurements in these plasmas. Thus, during each rotation, the $n = 1$ field effectively applied can vary by 100%. In other terms, we can expect that the helical core is here continuously switched on and off as the field rotates. On the other hand, when the B-coil field is larger, as in the cases discussed in previous sections, the impact on the mean profiles is present and even larger, but it is not significantly modulated in time. We note that all quantities shown in figure 6 recover when the $n = 1$ B-coil phase is around 0°, as indicated by the vertical dotted lines. This corresponds to the best error field correction phase, consistent with the error field measurements documented in [43].

In figure 7 the radial profiles of the various quantities introduced in figure 6 are compared at two times when the $n = 1$ error field is respectively

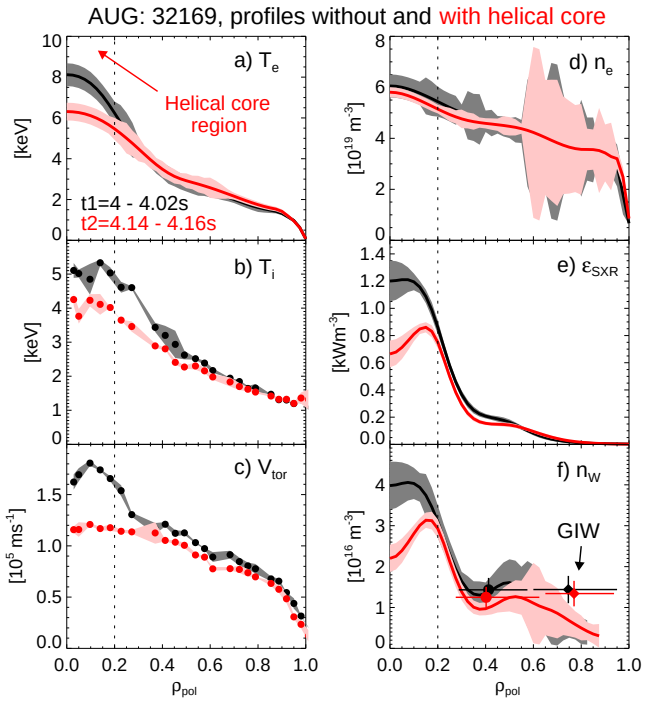

Figure 7. Radial profiles of the same quantities shown in figure 6 averaged in two time intervals when the helical core displacement is minimum (t_1, black) and maximum (t_2, red). These time intervals are also indicated in figure 6. The radial extent of the helical core is marked by a vertical dashed line.

minimized (black) and maximized (red). All profiles, with the only exception of the electron density one, are significantly reduced in the core region, $\rho_{pol} < 0.2$, while outer radii are much less affected. This corresponds to the region with largest helical core displacement, marked here with a vertical dotted line, as measured in similar discharges. A continuous $n = 3$ tearing mode rotating at $25 - 30kHz$ and radially localized around $\rho_{pol} \simeq 0.4$ is also present in this discharge. Its frequency follows the local plasma rotation, while its amplitude does not change significantly and it does not seem to be correlated with the $n = 1$ response modulation.

It is interesting to note that the W density is not only flattened, but a hole forms in the core when the helical core distortion is maximum. The W density is reconstructed here using soft x-ray and passive vacuum-ultraviolet measurements by a method described in [44]. Similar observations were recently made in ASDEX Upgrade for spontaneous 1/1 modes occurring in between sawteeth in standard H-mode plasmas [44, 45]. In both cases, axisymmetric transport modelling with the neoclassical code NEO [46] and the gyrokinetic code GKW [47], with the modelling approach of [48] and using the kinetic profiles shown in 7 as inputs, predicted equal peaking of W density at the two time slices, and consistent with the central peaking observed in the absence of helical core (time t_1). Thus the observed W hole can not be explained by axisymmetric transport effects and it is probably due to 3D effects.

Different mechanisms are candidates to explain these effects on the various profiles. The core electron and ion temperatures could be flattened by convective transport due to the double convective cell flow structure associated with the helical core, as proposed also for density and impurities in [49, 50]. Some magnetic stochasticity can not be completely excluded. Moreover, neoclassical non-ambipolar transport similar to stellarators could also play a role, since these plasmas have rather low collisionality and large helical ripple. Similarly, different braking mechanisms can possibly explain the effect on the rotation profile. In principle the W transport can also be affected by the mechanisms just mentioned. Initial investigations of neoclassical effects with the EUTERPE code were reported in [51]. Detailed transport modelling including 3D effects is underway for these experiments using EUTERPE and the drift-kinetic codes SFINCS [52] and NEO-2 [53, 54]. [The NTV torque is already available and is being included in a figure under preparation]

The above observations show that the core of high-β_N hybrid plasmas is very sensitive to external 3D fields. Error fields, if not properly minimized, could impact the core of hybrid plasmas. This is important to optimize the performance and to avoid excessive rotation braking that may lead to deleterious 2/1 modes. On the other hand, some finite level of asymmetry may be even beneficial to avoid W accumulation. Another possible solution to minimize helical core displacements could be to further elevate q_{min} above unity, though this requires additional current drive capabilities.

4. Spontaneous kink and tearing modes near no-wall limits

The ideal MHD plasma response does not only produce significant effects in presence of external 3D fields, with possible impact on the scenario. But even with a perfectly symmetric boundary, this sensitivity may affect internal MHD instabilities. In the example shown in figure 8, starting from a discharge similar to the ones analyzed above, a static $n = 1$ field is applied with B-coils to minimize the intrinsic error field and β_N is ramped using feedback control of the neutral beam power. When β_N reaches a value of about 2.6, slightly above the no-wall limit estimated by MARS-F, a β_N collapse is observed. This is due to an $n = 1$ rotating mode that appears and locks to the wall in

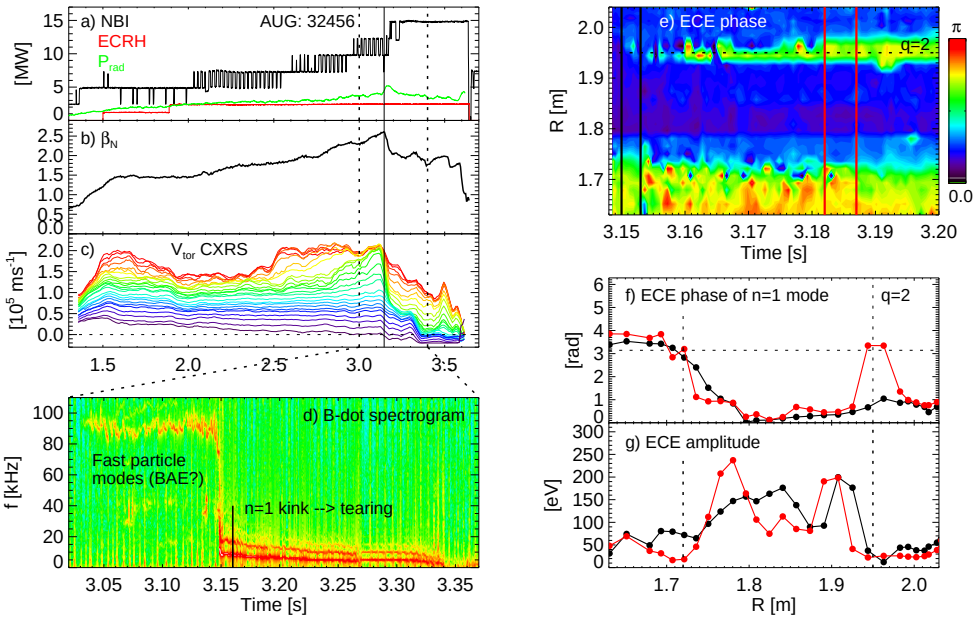

Figure 8. β_N ramp in an ASDEX Upgrade discharge with $n = 1$ error field correction using B-coils. (a) NBI, EC and radiated power. (b) β_N showing a collapse at $3.14s$. (c) Toroidal rotation at different radii. (d) Magnetic spectrogram across the β_N collapse, showing a series of fast particle-driven modes followed by an $n = 1$ mode that eventually locks to the wall. (e) ECE phase profiles at the $n = 1$ mode frequency. (f) ECE phase and (g) amplitude profiles just after the $n = 1$ mode appears (back) and when it develops an island at the $q = 2$ radius (red).

about $0.2s$. This mode appears after a sequence of fast particle-driven modes, possibly BAE modes, as seen in the magnetic spectrogram of figure 8(d), so it could be triggered by them or it could be linearly unstable. Analysis of fast ECE measurements show that the $n = 1$ mode starts as an ideal mode. This is evident from the profile of the relative phase between different ECE channels in figures 8(e) and (g): at the beginning the phase is rather flat, while after about $10ms$ a clear π-jump develops near the $q = 2$ radius, indicating the development of an island.

As anticipated above, as similar transition from kink to tearing parity was observed also in the discharge 32138 of figure 1, but in that case no clear trigger was present, while a large $n = 1$ field was applied possibly affecting the rotation profile. It is worth mentioning that other examples exist where β_N can be sustained in similar discharges for long periods at these β_N values or even larger [31]. The unstable case shown here does not represent a typical case in ASDEX Upgrade and it can not be used to identify a well defined limit, but it shows the possible consequences of an enhanced sensitivity of the plasma to both external and internal magnetic perturbations when β_N is raised near the no-wall limit. All techniques being developed to control tearing modes, for example by means of ECCD, can be used in these conditions.

5. Internal measurements of the helical core equilibrium in DIII-D hybrid plasmas

Experiments were conducted at DIII-D in high-β_N hybrid plasmas to study the effect of the $n = 1$ helical core distortion discussed above on the magnetic equilibrium, and in particular on the current density profile. Unique diagnostic capabilities were used to this aim, in particular a multi-channel MSE diagnostic that covers the plasma from the core to the edge. The 3D helical core equilibrium that forms is expected to redistribute central current density through a mechanism called flux pumping, based both on previous observations [8, 9] and recent modelling with nonlinear MHD codes [55, 56].

Flux pumping is a key mechanism to enable hybrid operation, in particular towards steady state conditions, since it can redistribute very efficiently large amounts of co-ECCD near the plasma center, where current drive efficiency is largest [10, 11]. The physics mechanisms ruling this effect are not yet completely understood, which would be necessary to extrapolate hybrid operation to future devices. An important open issue is whether temporal modulations of the MHD mode that provides flux pumping, typically a 3/2 tearing mode, are required, or if this mechanism can work even in stationary conditions. In standard hybrid operation, large modulations of the 3/2 amplitude provided by ELMs were in fact

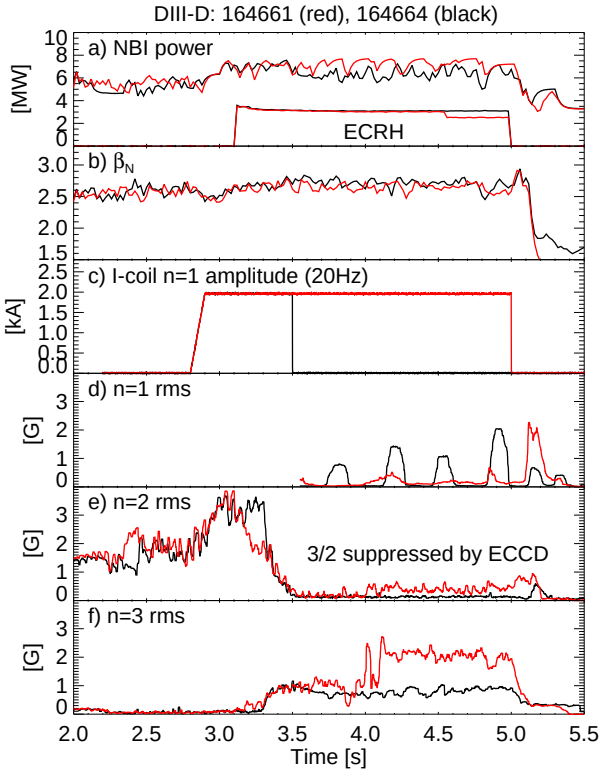

Figure 9. Two DIII-D hybrid discharges with the 3/2 tearing mode suppressed by ECCD and an $n = 1$ field rotating at $20Hz$ applied by the I-coils to induce a helical core. (a) NBI and ECRH power. (b) β_N feedback controlled by regulating the NBI power. Amplitude of (c) the $n = 1$, (d) $n = 2$, and (e) $n = 3$ rotating modes. When the $n = 1$ field is switched off (black), $n = 1$ sawtooth-like activity appears suggesting a loss of hybrid conditions.

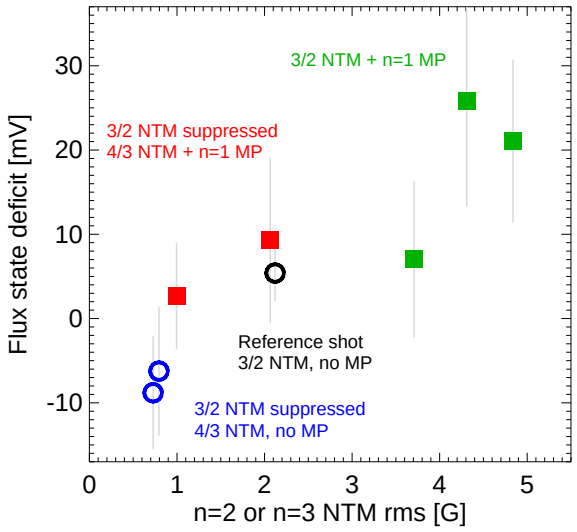

Figure 10. Flux state deficit, proportional to the amount of flux pumping, plotted as a function of the dominant mode amplitude for different DIII-D hybrid discharges: with and without 3/2 mode suppression, with and without $n = 1$ I-coil field applied. When the 3/2 mode is suppressed by ECCD, an $n = 3$ mode always appears.

shown to transiently enhance the amount of flux pumping maintaining it at a finite level [9]. So, an important question is whether this will work in ELM suppressed plasmas or not. The theory proposed in [55, 56] predicts that flux pumping can work in a stationary way, so experimental tests of this theory would represent an important step for the validation of the hybrid scenario.

Studying the impact of an externally induced helical core on the internal magnetic field equilibrium can give useful insights on flux pumping physics. Direct measurements of the internal magnetic field perturbations were done using MSE. These data were then used by the nonlinear 3D equilibrium code VMEC/V3FIT [28] to provide the first direct reconstruction of a helical core equilibrium in a tokamak [57].

Figure 9 introduces the experiment performed in DIII-D. Standard hybrid discharges at $\beta_N \simeq 3$ were used to measure the plasma response to slowly-rotating $(20Hz)$ $n = 1$ fields, similarly to what described above for ASDEX Upgrade. These plasmas have plasma current $I_P = 1.2MA$, toroidal field $B_T = -1.74T$, $q_{95} = 4.2$, and double null shape biased down. Since β_N is the main parameter that determines the $n = 1$ plasma response amplitude, NBI power is feedback controlled to maintain β_N constant under varying conditions, as show in figures 9(a) and (b). Note that the discharge duration was limited by NBI power availability, not by instabilities. To better isolate the effect of the induced $n = 1$ helical core with respect to the flux pumping effect normally provided by the 3/2 mode, this was suppressed with ECCD applied at the $q = 1.5$ surface starting from $3.1s$. Simultaneously a rotating $n = 1$ field is applied with the I-coils, two rows of 6 internal non-axisymmetric coils. An upper-to-lower I-coil phasing $\Delta\phi^{U/L} = 300deg$ was chosen to maximize the coupling with the edge harmonics of the $n = 1$ kink mode in the given equilibrium.

When the 3/2 mode is suppressed and no $n = 1$ fields are applied, as in the discharge 164664 shown in black in figure 9, an $n = 1$ mode with sawtooth-like behavior, rotating at the frequency of the plasma core, is reproducibly observed, as shown in figure 9(d). Similar observations were done before in DIII-D, with the return of sawtooth-like activity being attributed to lack of flux pumping to maintain the plasma in hybrid conditions [58]. When the $n = 1$ field is applied, as in the discharge 164661 shown in red in figure 9, a helical core distortion of a few cm forms, similar to what was observed in ASDEX Upgrade (evidence of this will be described in detail in the following). In this case

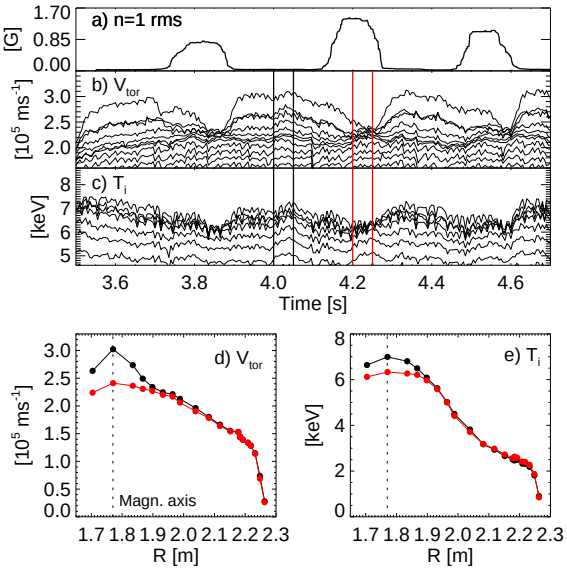

Figure 11. (a) Sawtooth-like $n = 1$ mode in DIII-D discharge 164664, with 3/2 mode suppressed by ECCD. (b) Toroidal rotation and (c) ion temperature time traces from central CXRS channels and (d,e) the radial profiles of the same quantities before and during an $n = 1$ sawtooth-like event.

the sawtooth-like activity is strongly suppressed and a low-amplitude continuous $n = 1$ mode remains. This suggests that the helical core distortion may provide some finite level of flux pumping that helps maintaining hybrid conditions. The situation is actually more complex: in fact a 4/3 mode spontaneously appears as the 3/2 mode is suppressed, as shown in figure 9(f). This is normally observed in DIII-D hybrid discharges when the 3/2 mode is suppressed or at relatively low β_N. Previous experiments showed that the flux pumping provided by 4/3 or 5/3 modes is normally lower than that produced by the 3/2 mode [9]. Nevertheless, the presence of this mode makes it more difficult to quantify the flux pumping provided by the $n = 1$ helical core alone.

Nevertheless, since the 4/3 mode is present both with and without the helical core, an attempt to quantify the amount of flux pumping present in both types of discharges was made, to isolate a difference between them. This was done using a technique described in [59], which was developed to track the consumption inside the plasma of poloidal flux provided by external coils. Since flux pumping can be thought as a conversion of toroidal into poloidal flux produced by a helical mode, this technique can be applied to this aim. Figure 10 shows the poloidal flux deficit estimated by this methods plotted as a function of the dominant tearing mode amplitude for various hybrid discharges: with and without 3/2 mode suppression, with and without the helical core induced by external $n = 1$ fields. In the discharges with the helical core present and the 3/2 mode suppressed (red squares), the flux deficit is on average higher than in cases without helical core (blue circles). This is true even if the $n = 3$ mode amplitude is significantly different in these two cases, which suggests that a finite level of flux pumping is likely provided by the helical core, though it remains difficult to measure its contribution with respect to the $n = 3$ one. Figure 10 also shows cases with the 3/2 mode present and an $n = 1$ field applied (green squares). They have larger flux deficit than the reference case with only a 3/2 mode (black circle), but they also have a larger 3/2 amplitude, which could explain the larger flux deficit. The reason why the 3/2 amplitude increases with the $n = 1$ field applied is not yet understood.

Figure 11 investigates more in detail the nature of the sawtooth-like modes observed in discharge 164664. Unfortunately no ECE measurements are available in these discharges since central channels are in cutoff. Nonetheless the ion temperature and rotation profiles measured by CXRS show a clear collapse localized in the core region when the $n = 1$ modes appear, which indicates that these events are very similar to regular sawteeth. In discharge 164661, with $n = 1$ fields applied, these crashes disappear and central CXRS channels only detect a $20Hz$ oscillation due to the forced rotation of the helical core.

Finally, figure 12 summarizes the experimental evidence and the reconstruction of the helical core equilibrium that forms in discharge 164661. Clear oscillations due to the forced rotation of the helical core are observed both in multi-chord soft x-ray and MSE measurements. Figures 12(a) to (d) show the amplitude and phase of these oscillations for both diagnostics (black dots). The soft x-ray chord geometry and the positions of the MSE channels are shown in panel (e). Similarly to what is observed in ASDEX Upgrade, two clear peaks are present in the core, where the phase has a π-jump that confirms the $m = 1$ character of the helical displacement.

These data were used as constraints to reconstruct the experimental 3D equilibrium with the code VMEC/V3FIT [28]. V3FIT iterates many VMEC runs, while minimizing a series of constraints, and it converges to a 3D equilibrium solution that best fits both axisymmetric and 3D measurements. The code was applied before to fit 3D equilibria in stellarators and reversed-field pinches [28]. This is its first application to a 3D helical core in a tokamak. More details on this work are being published in [57].

The soft x-ray and MSE data simulated by the synthetic diagnostics implemented in V3FIT are compared to the experimental profiles in figure 12, shown by a red line. Overall a good match is observed. The helical flux surfaces obtained by VMEC/V3FIT

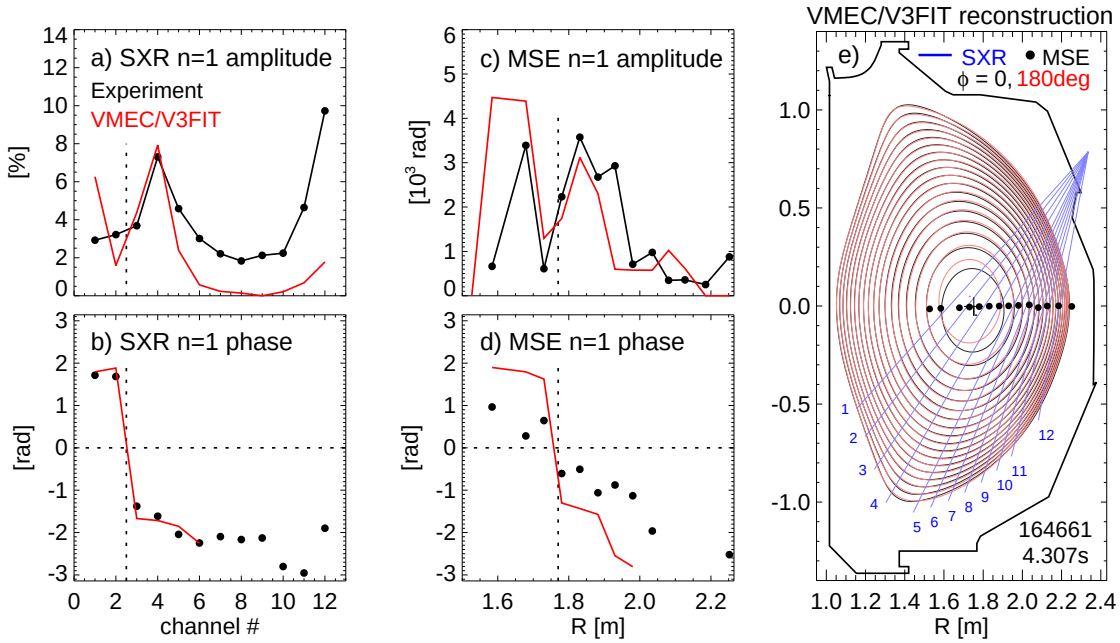

Figure 12. Radial profiles of the amplitude and phase of the $n = 1$ plasma response measured by (a,b) the difference of two toroidally-separated soft x-ray cameras and (c,d) a multi-channel MSE diagnostic in the DIII-D hybrid discharge 164661, with the 3/2 mode suppressed by ECCD and $n = 1$ field applied by I-coils to induce a helical core. (e) Helical flux surfaces of the 3D equilibrium reconstructed by VMEC/V3FIT using the soft x-ray and MSE measurements as constraints. The VMEC/V3FIT simulated data are shown in the previous panels by a red line.

are shown in figure 12(e). Two slices at the toroidal angles $\phi = 0°$ and $180°$ are shown in black and red, respectively. A $m = 1$ helical displacement of about $4cm$ is clearly visible in the core. Outer flux surfaces are also helically displaced, though the displacement value is lower. The safety factor profile obtained by VMEC/V3FIT is very close to 1 in the core (not shown here), which is typical of hybrid conditions.

The DIII-D experiments described above showed that the helical core probably contributes to flux pumping, though quantitative estimates are complicated by the presence of other MHD modes that could not be easily avoided. Ongoing work aims at calculating the effective loop voltage generated by the helical core distortion directly from the 3D equilibrium provided by VMEC/V3FIT, by balancing Ohm's law over the helical flux surfaces, in a way similar to that described in [55, 56].

6. Conclusions and future perspectives

In the present work, the impact that ideal MHD stability limits have on high-β_N hybrid operation was investigated in two large tokamaks like ASDEX Upgrade and DIII-D. This was done in particular by probing hybrid plasmas in these devices with rotating $n = 1$ fields applied by internal non-axisymmetric coils. Key to these studies was the capability of both devices to flexibly scan the poloidal spectrum of the applied field. The plasma response to external magnetic perturbations was measured with a wide suite of excellent diagnostics in both machines. They allowed to measure the full radial profile of the $n = 1$ displacement and its edge poloidal structure. The main result of these experiments is that the $n = 1$ plasma response in hybrid plasmas is by far largest in the plasma core, where it is dominated by the $m = 1$ harmonic. This behavior is due to the characteristic safety factor profile in these plasmas, with q_{min} just above 1. This feature makes the 1/1 harmonic very responsive to external 3D fields and allows the plasma to easily kink into a 3D helical core equilibrium as β_N is raised toward the no-wall limit.

These measurements qualitatively agree with MHD simulations done with the MARS-F and M3D-C^1 codes in ASDEX Upgrade, though the large 1/1 harmonic could not be satisfactorily reproduced. More precise measurements of the core q profile and/or additional physics beyond single-fluid MHD may be needed to reach quantitative agreement. These measurements are not only very useful to validate MHD codes, making our predictive capabilities more robust. They also made more clear the impact that 3D effects can have on the performance and stability of hybrid plasmas running at high-β_N close to, or even above the ideal MHD no-wall limit, as it will

be probably required in future machines to maximize fusion performance and allow steady state operation. In fact even small external 3D fields, which could be due for example to intrinsic error fields or that could be intentionally applied to mitigate ELMs, have their largest impact on the plasma core and can affect various plasma quantities. Helical core displacements of $1cm$ can significantly flatten the core electron and ion temperature and they can brake plasma rotation in present machines. Core rotation braking is certainly not beneficial, in particular in future devices like ITER and DEMO, where the NBI driven rotation is predicted to be low. We observe in fact that deleterious $n = 1$ modes are more easily triggered when core rotation is reduced below a certain threshold that corresponds approximately to half its initial value.

Interestingly, the helical core also has a clear impact on W transport, causing significant expulsion of W out of the core, in agreement with recent similar work in standard H-mode [44, 45]. This may be in principle beneficial and must be properly understood with dedicated modelling and experiments. These results indicate that the W hole that forms can not be explained by transport in an axisymmetric equilibrium and probably 3D effects play an important role. The physics of W transport in the helical core has interesting analogies with stellarators and in fact stellarators transport codes like EUTERPE [51], SFINCS [52], and NEO-2 [53, 54] are presently being used to try and explain these observations.

External 3D fields are not only a way to probe the stability limits of hybrid plasmas. They were also useful to investigate an interesting physics mechanism that is essential for the functioning of the hybrid scenario. DIII-D experiments not only confirmed the helical core observation made in ASDEX Upgrade. They also gave an insight in the physics of flux pumping, by which MHD modes can redistribute current density out of the core, making hybrid operation possible. This mechanism can efficiently redistribute significant amounts of co-ECCD driven near the core, thus enabling steady state hybrid operation.

Acknowledgments

This work has been carried out within the framework of the EUROfusion Consortium and has received funding from the Euratom research and training programme 2014-2018 under grant agreement No 633053. The views and opinions expressed herein do not necessarily reflect those of the European Commission.

References

[1] Gruber O *et al* 1999 *Phys. Rev. Lett.* **83** 1787
[2] Luce T C *et al* 2001 *Nucl. Fusion* **41** 1585
[3] Sips A C C *et al* 2002 *Plasma Phys. Control. Fusion* **44** B69
[4] Joffrin E *et al* 2003 *Plasma Phys. Control. Fusion* **45** A367
[5] Gruber O *et al* 2009 *Nucl. Fusion* **49** 115014
[6] Oyama N *et al* 2009 *Nucl. Fusion* **49** 065026
[7] Luce T C *et al* 2014 *Nucl. Fusion* **54** 013015
[8] Politzer P A *et al* 2005 Proceedings of the 32nd European Conference on Plasma Physics, Tarragona **29C** O-1.001
[9] Petty C C *et al* 2009 *Phys. Rev. Lett.* **102** 045005
[10] Turco F *et al* 2015 *Phys. Plasmas* **22** 056113
[11] Petty C C *et al* 2016 *Nucl. Fusion* **56** 016016
[12] Boozer A H 2001 *Phys. Rev. Lett.* **86** 5059
[13] Callen J D 2011 *Nucl. Fusion* **51** 094026
[14] Brennan D P *et al* 2003 *Phys. Plasmas* **10** 1643
[15] Brennan D P *et al* 2007 *Phys. Plasmas* **14** 056108
[16] Günter *et al* 2001 *Nucl. Fusion* **41** 1283
[17] Ferron J R *et al* 2005 *Phys. Plasmas* **12** 056126
[18] Garofalo A M *et al* 2006 *Phys. Plasmas* **13** 056110
[19] Chapman I T *et al* 2009 *Plasma Phys. Control. Fusion* **51** 055015
[20] Chu M S and Okabayashi M 2010 *Plasma Phys. Control. Fusion* **52** 123001
[21] Igochine V 2012 *Nucl. Fusion* **52** 074010
[22] Garofalo A M 2015 *Nucl. Fusion* **55** 123025
[23] ASDEX Upgrade Team 2003 *Fusion Sci. Technol.* **44** 1
[24] Luxon J L and Davis L G 1985 *Fusion Technol.* **8** 441
[25] Liu Y Q *et al* 2000 *Phys. Plasmas* **7** 3681
[26] Ferraro N M and Jardin S C 2009 *J. Comput. Phys.* **228** 7742
[27] Hirshman S P and Whitson J C 1983 *Phys. Fluids* **26** 3554
[28] Hanson J D *et al* 2009 *Nucl. Fusion* **49** 075031
[29] Suttrop W *et al* 2009 *Fusion Eng. Des.* **84** 290
[30] Rott M *et al* 2009 *Fusion Eng. Des.* **84** 1653
[31] Bock A *et al* 2016 Proceedings of the 43^{rd} European Conference on Plasma Physics, Leuven, O3.110
[32] Mc Carthy P J 1999 *Phys. Plasmas* **6** 3554
[33] Hawryluk R J 1980 *Physics of Plasmas Close to Thermonuclear Conditions*, edited by B. Coppi CEC, Brussels, Vol. 1, pp. 1946
[34] Rathgeber S K *et al Plasma Phys. Control. Fusion* **55** 025004
[35] Piovesan P *et al* 2015 EPS 2015
[36] Buratti P *et al* 2006 *Plasma Phys. Control. Fusion* **48** 1005
[37] Buratti P *et al* 2012 *Nucl. Fusion* **52** 023006
[38] Chapman I T *et al* 2010 *Nucl. Fusion* **50** 045007
[39] Liu Y *et al* 2008 *Phys. Plasmas* **15** 112503
[40] Ford O P *et al* 2016 *Imaging motional stark effect measurements at ASDEX Upgrade* 21st Topical Conference on High Temperature Plasma Diagnostics
[41] Mlynek A *et al* 2016 *First results from the new submillimeter polarimeter on the ASDEX Upgrade tokamak* 21st Topical Conference on High Temperature Plasma Diagnostics
[42] Weiland M *et al* 2015 *Plasma Phys. Control. Fusion* **57** 085002
[43] Maraschek M *et al* 2013 Proceedings of 40^{th} EPS Conference on Plasma Physics, Espoo, P4.127
[44] Sertoli M *et al* 2015 *Plasma Phys. Control. Fusion* **57** 075004
[45] Sertoli M *et al* 2015 *Nucl. Fusion* **55** 113029
[46] Belli E A and Candy J 2012 *Plasma Phys. Control. Fusion* **54** 015015
[47] Peeters A G *et al* 2009 *Comput. Phys. Commun.* **180** 2650
[48] Angioni C *et al* 2014 *Nucl. Fusion* **54** 083028
[49] Nicolas T *et al* 2012 *Phys. Plasmas* **19** 112305
[50] Nicolas T *et al* 2014 *Phys. Plasmas* **21** 012507
[51] García-Regaña J M *et al* 2015 *42nd EPS Conference on Plasma Physics* paper P2.170
[52] Landreman M *et al* 2014 *Phys. Plasmas* **21** 042503

[53] Kernbichler W *et al* 2008 *Plasma and Fusion Research* **3** S1061-1
[54] Kasilov S V *et al* 2014 *Phys. Plasmas* **21** 092506
[55] Bonfiglio D *et al* 2005 *Phys. Rev. Lett.* **94** 145001
[56] Jardin S C *et al* 2015 *Phys. Rev. Lett.* **115** 215001
[57] Cianciosa M *et al* paper in preparation
[58] Wade M R *et al* 2005 *Nucl. Fusion* **45** 407
[59] Luce T C *et al* 2014 *Nucl. Fusion* **54** 903005
[60] St. John H E *et al* 1995 Proceedings of 15^{th} IAEA Fusion Energy Conference on Plasma Physics and Controlled Nuclear Fusion Research IAEA, Vienna **3** 60